Electronic Supplementary Material (ESI) for Materials Advances.

Pressure effect on long-term heat storage ceramics based on Mg-substituted λ-Ti_3O_5

Shin-ichi Ohkoshi,[1,*] Fangda Jia,[1] Marie Yoshikiyo,[1] Kenta Imoto,[1] Hiroko Tokoro,[1,2] Kosuke Nakagawa,[1] Yuta Maeno,[1] Asuka Namai,[1] Risa Harada,[3] Kenji Hattori,[3] Kunihiro Kojima,[3] Kei Sugiura,[3] and Takatoshi Suganuma[3]

[1] *Department of Chemistry, School of Science, The University of Tokyo, 7-3-1 Hongo, Bunkyo-ku, Tokyo 113-0033, Japan*

[2] *Division of Materials Science, Faculty of Pure and Applied Sciences, University of Tsukuba 1-1-1 Tennodai, Tsukuba, Ibaraki 305-8577, Japan*

[3] *Denso Corporation, 1-1 Showa-cho, Kariya, Aichi 448-8661, Japan*

Table of Contents:

Section 1. Crystal structure analyses

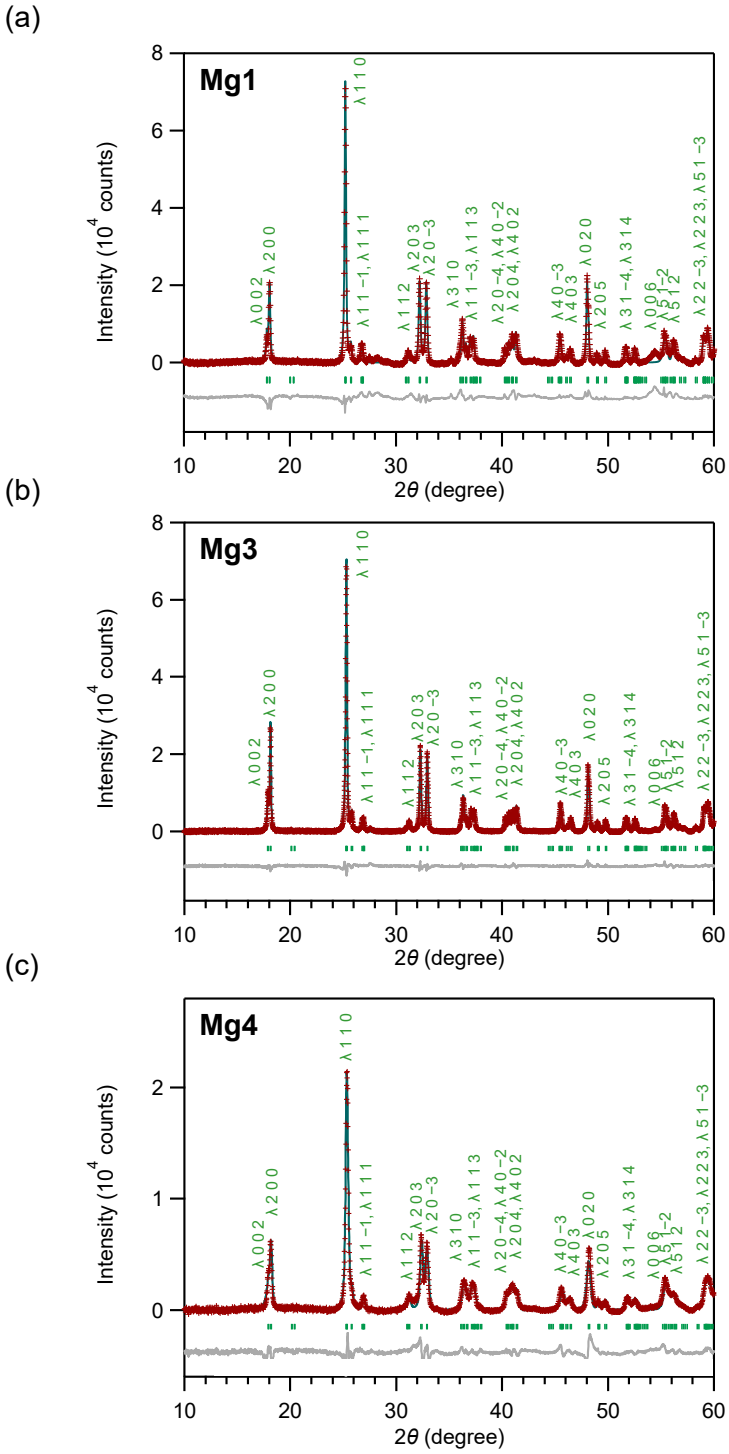

Fig. S1 | PXRD patterns with Rietveld analysis of (a) **Mg1**, (b) **Mg3**, and (c) **Mg4** under atmospheric pressure (0.1 MPa). Red plots, black line, and gray line are the observed pattern, the total calculated pattern, and the residual pattern, respectively. Green bars represent the calculated positions of the Bragg reflections.

Table. S1 | Crystal structural parameters of λ-$Mg_xTi_{3-x}O_5$ obtained by Rietveld refinement of the PXRD patterns of **Mg1**–**Mg4**.

		Mg1	**Mg2**	**Mg3**	**Mg4**
		λ-$Mg_{0.015}Ti_{2.985}O_5$	λ-$Mg_{0.022}Ti_{2.978}O_5$	λ-$Mg_{0.043}Ti_{2.957}O_5$	λ-$Mg_{0.053}Ti_{2.947}O_5$
a (Å)		9.8286(9)	9.8357(2)	9.8284(4)	9.8155(3)
b (Å)		3.7875(2)	3.78584(4)	3.78733(8)	3.78565(6)
c (Å)		9.9676(9)	9.9712(2)	9.9709(3)	9.9680(2)
β (°)		91.173(4)	91.1946(11)	91.094(2)	90.950(2)
V (Å^3)		370.97(5)	371.211(10)	371.08(2)	370.340(14)
R_{wp}		5.527	2.514	4.902	4.074
S		5.0778	1.9383	1.5528	2.8119
Occupancy of Mg (%)	Ti1	0	0	0	0
	Ti2	1.5	2.2	4.3	5.3
	Ti3	0	0	0	0
Ti1	*x*	0.6284(5)	0.62963(12)	0.6329(3)	0.6259(5)
	y	0	0	0	0
	z	0.0531(4)	0.05274(11)	0.0538(3)	0.0559(5)
Ti2	*x*	0.3044(3)	0.30465(9)	0.3047(2)	0.3040(4)
	y	0	0	0	0
	z	0.2435(5)	0.24542(12)	0.2451(2)	0.2449(6)
Ti3	*x*	0.6351(4)	0.63473(12)	0.6356(3)	0.6323(5)
	y	0	0	0	0
	z	0.4337(4)	0.43492(10)	0.4344(2)	0.4343(5)
O1	*x*	0.445(2)	0.4506(4)	0.4486(9)	0.455(2)
	y	0	0	0	0
	z	0.3919(12)	0.3882(3)	0.3862(7)	0.3900(14)
O2	*x*	0.1686(14)	0.1812(3)	0.1778(8)	0.193(2)
	y	0	0	0	0
	z	0.0659(13)	0.0650(3)	0.0694(8)	0.0693(15)
O3	*x*	0.7306(12)	0.7377(3)	0.7365(7)	0.7273(12)
	y	0	0	0	0
	z	0.2522(12)	0.2499(3)	0.2540(7)	0.2493(15)
O4	*x*	0.5441(14)	0.5467(4)	0.5418(9)	0.544(2)
	y	0	0	0	0
	z	0.8654(12)	0.8731(3)	0.8706(7)	0.8824(13)
O5	*x*	0.1857(14)	0.1896(4)	0.1785(9)	0.177(2)
	y	0	0	0	0
	z	0.4306(12)	0.4290(3)	0.4306(8)	0.4323(13)

Section 2. Temperature changes due to the applied pressure

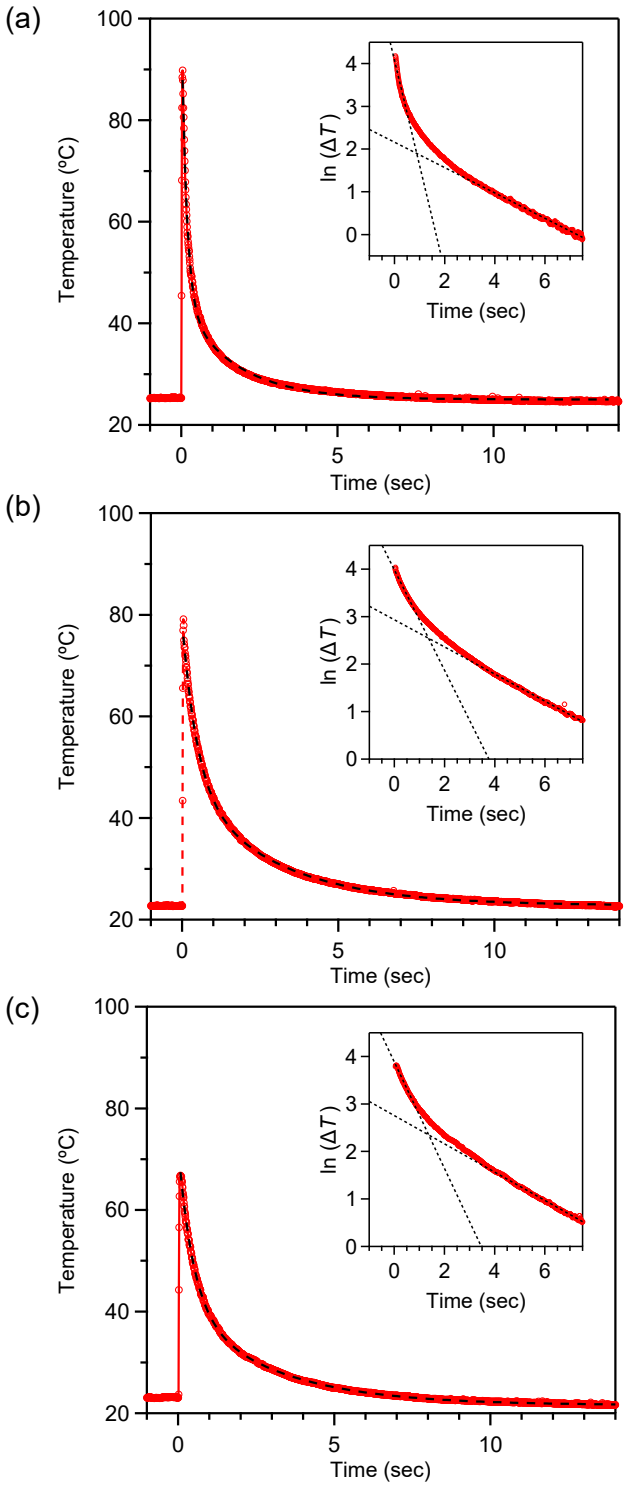

Fig. S2 | Decay of the maximum temperature within a square area after applying pressure to the samples at t = 0 for (a) **Mg1**, (b) **Mg2**, and (c) **Mg4**. Dotted lines are the fitting results of a double exponential function, $\Delta T = A_1\exp(-t/\tau_1) + A_2\exp(-t/\tau_2)$, where ΔT is the temperature change, t is time, τ_1 and τ_2 are decay times, and A_1 and A_2 are constants.

Section 3. Variable-temperature PXRD measurements

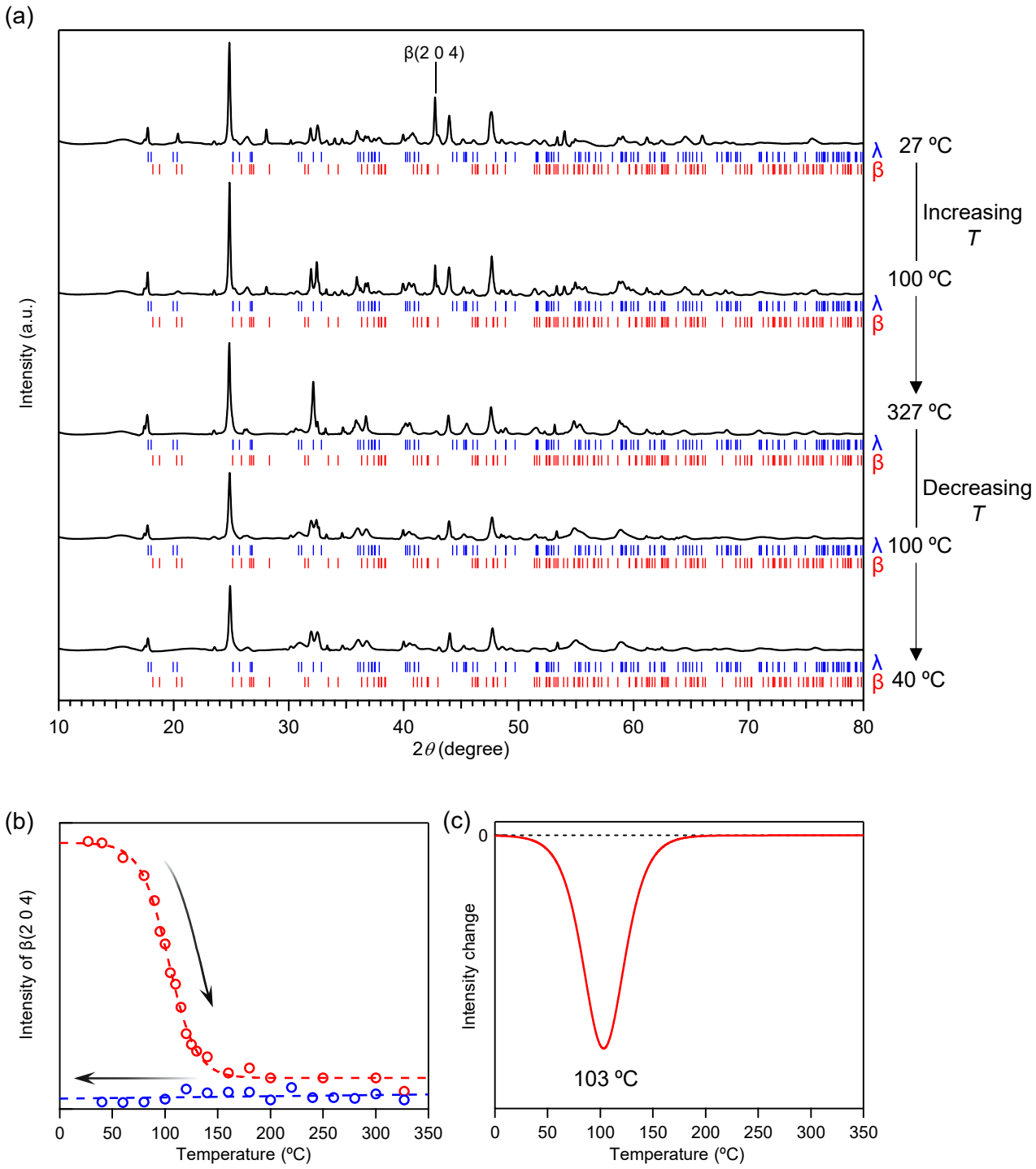

Fig. S3 | Variable-temperature PXRD measurement of **Mg3**. Change in the β-phase characteristic peak (2 0 4) in Miller index is emphasized in (a) the temperature-dependent PXRD. The Hill equation (red dashed line) is fitted to the area below the β (2 0 4) peak in the temperature-increasing process (red), a line (blue dashed line) is fitted to the temperature-decreasing process (blue) as shown in (b). (c) Derivative of the fitted Hill equation (red solid line). Shape is assumed to reproduce the DSC pattern.

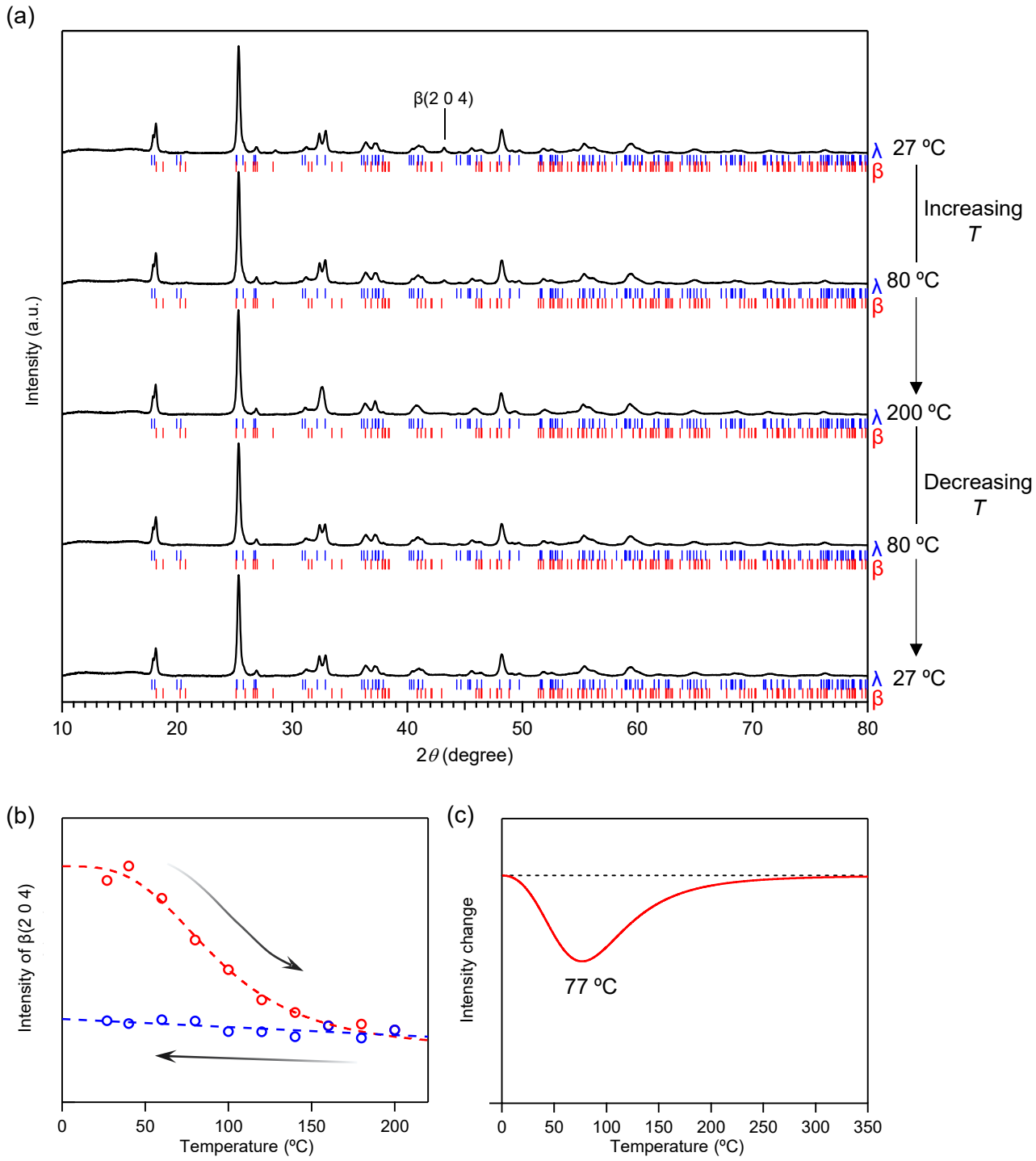

Fig. S4 | Variable-temperature PXRD measurement of **Mg4**. Change in the β-phase characteristic peak (2 0 4) in Miller index is emphasized in (a) the temperature-dependent PXRD. The Hill equation (red dashed line) is fitted to the area below the β (2 0 4) peak in the temperature-increasing process (red), a line (blue dashed line) is fitted to the temperature-decreasing process (blue) as shown in (b). (c) Derivative of the fitted Hill equation (red solid line). Shape is assumed to reproduce the DSC pattern.

Section 4. SD-model calculations under external pressure

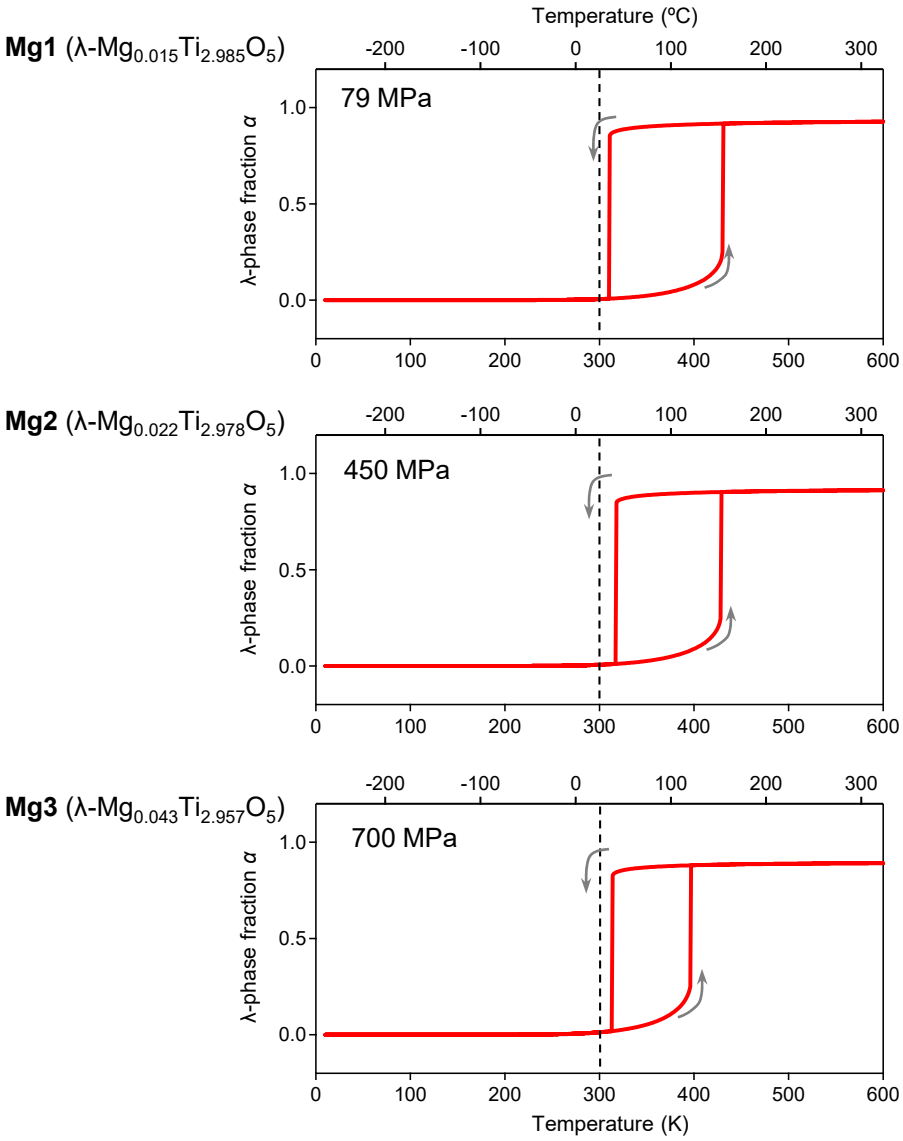

Fig. S5 | λ-phase fraction versus temperature plot under external pressure simulated by SD model calculations.

Section 5. TEM images and primary size distributions

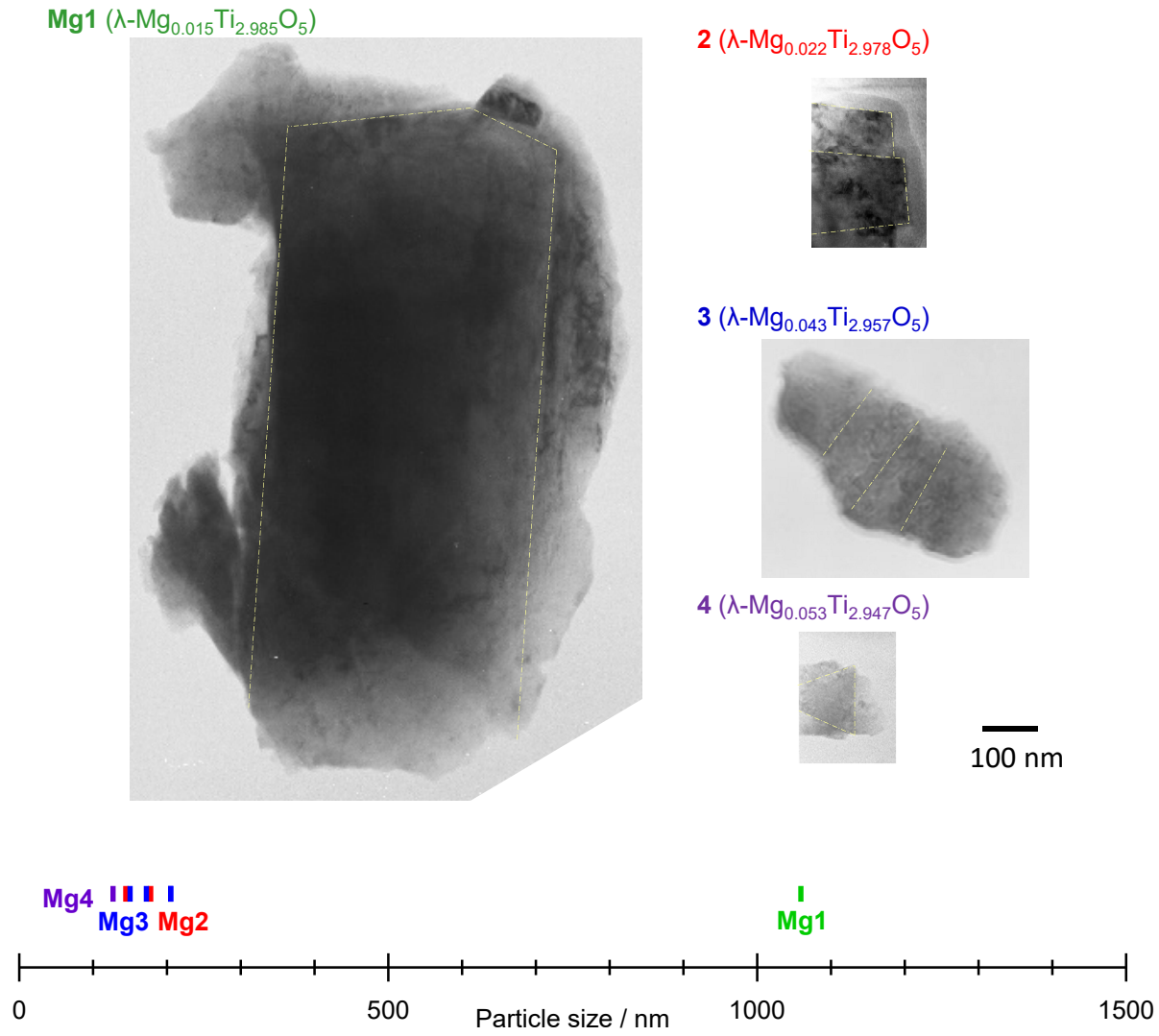

Fig. S6 | TEM images of **Mg1**, **Mg2**, **Mg3**, and **Mg4**. Yellow dotted lines indicate the boundaries of the primary domains. Bottom figure shows the primary size distributions.

Section 6. Curie component of λ-$Mg_xTi_{3-x}O_5$

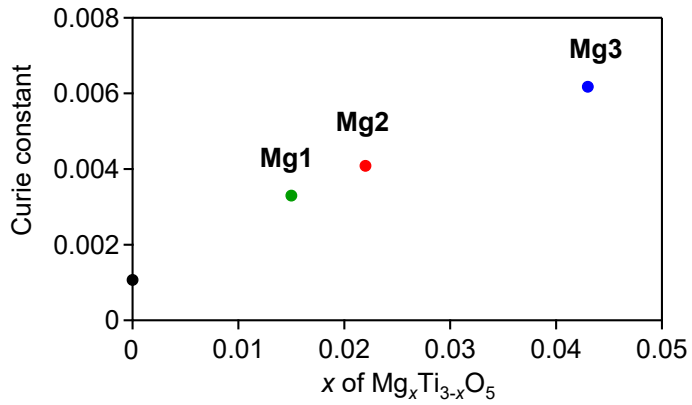

Fig. S7 | Curie component of λ-$Mg_xTi_{3-x}O_5$. The x value dependence of the Curie constants, which were obtained by fitting the low temperature region of the magnetic susceptibility data based on Curie's law [$\chi = C/T$ (C: Curie constant)]. Black circle shows the data adapted from ref. 15.